

# Impact of Many-Body Correlations on the Dynamics of an Ion-Controlled Bosonic Josephson Junction

J. M. Schurer,<sup>1,2,\*</sup> R. Gerritsma,<sup>3</sup> P. Schmelcher,<sup>1,2</sup> and A. Negretti<sup>1,2</sup>

<sup>1</sup>*Zentrum für Optische Quantentechnologien, Universität Hamburg,  
Luruper Chaussee 149, 22761 Hamburg, Germany*

<sup>2</sup>*The Hamburg Centre for Ultrafast Imaging, Universität Hamburg,  
Luruper Chaussee 149, 22761 Hamburg, Germany*

<sup>3</sup>*Institut für Physik, Johannes Gutenberg-Universität Mainz, 55099 Mainz, Germany*

(Dated: November 6, 2018)

We investigate an atomic ensemble of interacting bosons trapped in a symmetric double well potential in contact with a single tightly trapped ion which has been recently proposed [R. Gerritsma *et al.*, Phys. Rev. Lett. **109**, 080402 (2012)] as a source of entanglement between a Bose-Einstein condensate and an ion. Compared to the previous study, the present work aims at performing a detailed and accurate many-body analysis of such combined atomic quantum system by means of the ab-initio multi-configuration time-dependent Hartree method for bosons, which allows to take into account all correlations in the system. The analysis elucidates the importance of quantum correlations in the bosonic ensemble and reveals that entanglement generation between an ion and a condensate is indeed possible, as previously predicted. Moreover, we provide an intuitive picture of the impact of the correlations on the out-of-equilibrium dynamics by employing a natural orbital analysis which we show to be indeed experimentally verifiable.

PACS numbers: 34.50.Cx, 67.85.De, 37.10.Ty, 31.15.-p

## I. INTRODUCTION

In the past five years, the interest in combining ultracold atoms and ions has tremendously grown, especially after the first experimental attempts [1–3] in reaching the ultra-cold regime in such hybrid atomic quantum system. Theoretical studies on the subject, however, have been carried out already before those experiments, for instance, for investigating related scattering properties [4, 5] or the formation of molecular ions in a Bose-Einstein condensate (BEC) [6]. Although not so much appreciated and probably not so known, this fascinating topic has already attracted the interest of Eugene Gross in the early sixties [7]. He was mainly interested in the estimation of the effective mass of a moving ion and in its impact on the ensemble of weakly repulsive bosonic particles in the condensate state. Gross’s investigations were mostly motivated by experiments carried out at that time with positive and negative ions in liquid helium, and the goal was to develop a systematic theory starting from first principles, without invoking experimental data, in order to explain the large effective mass observed in corresponding low temperature experiments. More recently, however, the combination of different atomic systems like neutral atoms and ions, Rydberg atoms or polar molecules has open a new avenue in the research of ultracold quantum matter. Indeed, such hybrid quantum systems of ultracold atoms, especially atom-ion systems, offer a new laboratory in order to investigate ultracold chemistry and its related phenomena such as

the formation of chemical bonds, charge exchange and transport. Furthermore, because of their superb controllability, combined systems of atoms and ions represent a promising platform for the study of condensed-matter phenomena like polarons [8–10], the Kondo effect [11], charge density waves [12], and for the design of novel many-body quantum states. From a more genuine atomic perspective, the study of such atom-ion systems enables the investigation of efficient (sympathetic) cooling schemes for ions and atoms, entanglement generation and its propagation in the combined system (see, for instance, Ref. [13] for a review on the subject).

From a many-body theory point of view, most of the current studies concerning an impurity in a condensate are based on approximate models like mean-field theory [7], perturbative treatments [14, 15], or field-theoretical methods within the so-called ladder approximation [16]. An interesting example for a phenomenon which can not be described in a Gross-Pitaevskii (GP) framework is the ionization, for instance, of a Rydberg atom in a BEC and the subsequent dynamics, e.g. the capturing of atoms by the ion forming mesoscopic molecular ions [6]. The new length scale induced by the long-range atom-ion interaction plays a crucial role in the static as well as dynamical properties of the quantum gas. Very recently, theoretical studies of a single impurity immersed in a BEC employing ab-initio methods like quantum Monte Carlo [17] or the multi-configuration time-dependent Hartree method for bosons (MCTDHB) [18, 19] have been initiated. In particular, in Refs. [18, 19] the static as well as the dynamical properties of a single trapped ion in a quasi one-dimensional Bose gas in different regimes of atom-atom interactions have been explored. These investigations have clearly

---

\* jschurer@physnet.uni-hamburg.de

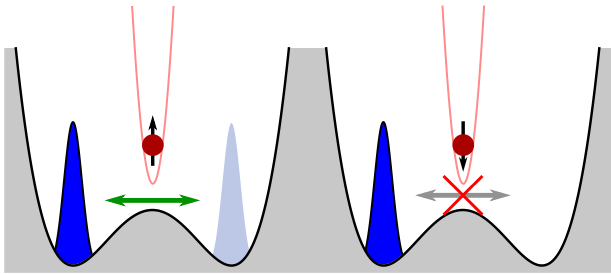


FIG. 1. Setup of a bosonic Josephson junction controlled by a spatially localized ion in the weak link of the junction. In dependence of the internal spin state of the ion, the atomic ensemble can either tunnel (left panel) or is self-trapped (right panel).

shown the necessity to use more advanced methods in order to accurately describe the ground and excited states of the gas as well as its dynamical evolution. A simple mean-field description of such system would yield an incomplete picture of the involved physics.

Motivated by these early studies and future perspectives, we analyze here in detail the many-body physics of an ensemble of bosonic particles in a symmetric double well potential whose tunneling is controlled by the internal spin state of a single tightly trapped ion such that the motion of the latter can be completely neglected (see Fig. 1). This setup represents essentially a controlled bosonic Josephson junction (BJJ). The BJJ of an atomic gas in a double well, and especially the occurrence of the macroscopic quantum self-trapping effect [20, 21], represents a paradigmatic example of a many-body phenomenon, where the role played by the repulsive interatomic interactions is of paramount importance [22–24]. The above setup, originating from Refs. [25, 26], goes one step further: by adding a single ion in the weak link of the junction (i.e., at the barrier position, see also Fig. 1), the control of the atom-ion collisions can be used to steer the BJJ dynamics and to generate entanglement between the ion and the condensate. In particular, in Ref. [25] it has been shown that the atom-ion scattering parameters can be chosen in such a way that either the tunneling regime (TR) or the self-trapping regime (STR) can be induced upon the internal state of the ion, and therefore entanglement between the two systems can be produced. Moreover, an experimentally feasible entanglement protocol has been proposed and validated both for a single ion and a single atom and for an ion and a small condensate - the latter within a two-mode Bose-Hubbard (TMBH) approach (see also Ref. [27]). Let us also note that such a hybrid BJJ can be also thought as a basic building block of a solid-state quantum simulator [12].

In the present work, we are precisely interested in the question whether the control of the BJJ remains possible in a many-body framework (i.e., beyond mean field) with the aim of understanding if beyond mean-field effects are relevant in the BJJ dynamics, how they affect the temporal evolution of the TR and the STR, or if not

to which extend the common two-mode Gross-Pitaevskii (TMGP) description is applicable. Moreover, we want to study the impact of the quantum correlations on the entanglement protocol in order to test the validity of the TMBH approximation employed in the original proposal [25]. We find that the control of the BJJ by the ion is indeed possible such that both dynamical regimes (i.e., TR and STR) can be observed. Correlations build-up in the course of the temporal evolution and lead to the population of more than a single mode (i.e., orbital) rendering the TMGP approximation inadequate and a TMBH description questionable, especially at longer times. Nevertheless, we show that the general entanglement protocol remains valid in its essence because the build-up of correlations takes place on a longer time scale than the relatively short one needed for the creation of the entangled state. Furthermore, we also conclude that the description of the entanglement protocol via a TMBH description is valid, but only if two time-dependent mode functions (i.e., orbitals) are chosen.

This work is organized as follows: In Sec. II we introduce the setup, thus, the model potential for the description of the atom-ion interaction and the many-body Hamiltonian. Here also the scattering properties of the two spin states of the ion are defined. Section III contains a detailed investigation of the dynamics of the bosonic ensemble for both internal ion states starting from the single-particle to the fully quantum correlated description. We end this section with brief considerations about experimental strategies to measure the impact of correlations. Afterwards, the validity of the entanglement protocol, if quantum correlations are taken into account, is analyzed in Sec. IV. Our analysis is completed in Sec. V by a discussion of a possible experimental realization. Finally, the relevant findings and conclusions are summarized in Sec. VI.

## II. MODEL AND THEORETICAL APPROACH

In this section, we introduce the hybrid double well setup under consideration and the atom-ion interaction which acts as the controllable “switch” for the dynamics of the atoms. In addition to this, we outline the MCT-DHB method used for the simulations.

### A. Model System

The atom-ion interaction, originating from the interplay between the charge of the ion and the induced dipole moment of the atom, scales in three dimensions (3D) like  $-ae^2/r^4$  with  $r$  the distance between the atom and the ion,  $a$  the static polarizability of the atom, and  $e$  the elementary charge. Let us note that even under strong transversal confinement, leading effectively to a quasi-1D motion, this interaction maintains its long-range behavior and its 1D form ( $-ae^2/z^4$ ) is valid up to some in-

ner cutoff distance [5]. Furthermore, it has been shown that the atom-ion scattering, exactly solvable by (multi-channel) quantum defect theory [28–32], can be approximated by the following model for the interaction potential [18]

$$V_{\text{ion}}(z) = v_0 e^{-\gamma z^2} - \frac{1}{z^4 + 1/\omega}, \quad (1)$$

which is very well-suited for our many-body investigations. Here  $z$  is the atom-ion relative coordinate  $z = z_A - z_I$ . The parameters of the model potential  $\gamma, \omega$  can be mapped onto the quantum defect parameters  $\varphi_e$  and  $\varphi_o$  [18] which uniquely determine the scattering behavior [5]. The Gaussian height ( $v_0 = 3\omega$ ) is chosen such that a node is enforced at  $z = 0$  which mimics the short-range behavior of the scattering solutions. Since the ion is meant to control the BJJ, we assume it to be localized in the weak link of the junction (see Fig. 1) and tightly trapped such that its motion can be neglected. We note that the above interaction induces a length ( $R^* = \sqrt{\alpha e^2 m / \hbar^2}$ ) and energy [ $E^* = \hbar^2 / (2mR^{*2})$ ] scale for the atoms of mass  $m$  and hereafter we use them to rescale the Hamiltonian.

Given this, the system of  $N$  bosonic atoms in a Josephson junction with an ionic switch can be described by the Hamiltonian

$$\hat{H} = \sum_{i=1}^N \underbrace{\left[ -\frac{\partial^2}{\partial z_i^2} + V_{\text{dw}}(z_i) + V_{\text{ion}}(z_i) \right]}_{\hat{h}} + g \sum_{i < j}^N \delta(z_i - z_j). \quad (2)$$

Here the Josephson junction is modeled by a double well potential of the form

$$V_{\text{dw}}(z) = \frac{b}{q^4} (z^2 - q^2)^2 \quad (3)$$

with  $b$  the barrier height and  $2q$  the distance between the wells. This trap is designed such that  $V_{\text{dw}}(0) = b$  and  $V_{\text{dw}}(\pm q) = 0$ . It can be approximated near the zero points by a harmonic potential  $V_{\text{dw}}^{\pm q}(z) = \frac{1}{2}m\omega_q^2(z \mp q)^2$  with  $\hbar\omega_q = 4\sqrt{b}/q$ . In addition, the interaction among the atoms is of short range character and can therefore be expressed as a contact delta interaction of strength  $g$ .

For later use, we introduce a single-particle basis set  $\{\phi_j(z)\}$  as eigenfunctions of the operator  $\hat{h}$

$$\hat{h}\phi_j(z) = \epsilon_j \phi_j(z) \quad (4)$$

with eigenenergies  $\epsilon_j$ . The corresponding creation and annihilation operators are defined as  $\hat{a}_j^\dagger$  and  $\hat{a}_j$ , respectively.

A frequently employed approach to the dynamics of  $N$  interacting bosons in a double well is the Gross-Pitaevskii equation, where the order parameter is expanded onto two single-particle mode functions  $|L\rangle$  and  $|R\rangle$  localized

in either well of the double well potential [20]. This model features two main dynamical regimes: the tunneling regime in which the atom cloud oscillates between the left and the right well and the self-trapping regime where most of the atomic ensemble remains trapped on one side of the well due to the interatomic interaction. The transition between the two regimes is characterized by the parameter  $\Lambda$

$$\Lambda = \frac{UN}{2J} \quad (5)$$

which contains the on-site interaction  $U = g \int |z|L\rangle|^4 dz$ , and the tunneling rate  $J = \langle L|\hat{h}|R\rangle$ . A critical value  $\Lambda_c$ , separating the tunneling ( $\Lambda < \Lambda_c$ ) and the self-trapping ( $\Lambda > \Lambda_c$ ) regime, has been derived [20]. Starting with the initial condition that all atoms are in one well, we obtain  $\Lambda_c = 2$ . This critical value allows us to determine either a critical interaction strength  $g_c$  or a critical particle number  $N_c$ . Beyond that, it is known (see Ref. [27]) that in the TR the tunneling frequency decreases with increasing  $\Lambda$ , at the critical value it becomes zero, but it increases again for  $\Lambda \gg \Lambda_c$ , even though only very incomplete tunneling takes place.

Ignoring the ion for a moment, we choose for the entire paper the double well parameters such that the bosonic ensemble is in the STR with  $gN = 0.2E^*R^*$  (see discussion of parameters in Sec. V). Note that the scaling of  $g$  with the particle number is chosen such that  $\Lambda$  is independent of  $N$  [see Eq. (5)] rendering the results independent of the particle number (at least within a TMGP description). In order to allow for the ion to switch the BJJ, we further choose  $\Lambda$  near, but larger than, its critical value  $\Lambda = 3.34 > \Lambda_c$  leading to  $q = 2.1R^*$  and  $b = 5.5E^*$ . With this choice the tunneling constant  $J$  is large enough while the overlap  $\langle L|R\rangle$  is still small. The corresponding potential is shown in Fig. 2 (left panel).

Adding the ion, the objective is now to find two sets of quantum defect parameters, corresponding to two different short-range scattering behaviors such that in one case the atoms can tunnel through the junction and in the other they remain self-trapped. The quantum defect parameters can be chosen as  $\varphi_e^{\text{TR}} = 0.23\pi$ ,  $\varphi_o^{\text{TR}} = -0.45\pi$  for the TR and as  $\varphi_e^{\text{STR}} = 0.23\pi$ ,  $\varphi_o^{\text{STR}} = 0.3\pi$  for the STR. This choice corresponds to  $\omega = 29(R^*)^{-4}$  and  $\gamma = 10\gamma_{\text{min}}$  in the TR leading to an interaction parameter  $\Lambda_{\text{TR}} = 0.68$  and to  $\omega = 80(R^*)^{-4}$  and  $\gamma = \gamma_{\text{min}}$  for the STR corresponding to  $\Lambda_{\text{STR}} = 4.50$  with  $\gamma_{\text{min}} = 4\sqrt{10}\omega$ . Note, that this choice of model parameters results in two bound states in the atom-ion interaction potential.

In order to understand this choice of parameters or, in other words, which property is relevant for the switching behavior, we look at Fig. 2. While the two double well modes  $|L\rangle$  and  $|R\rangle$  in the right panel show almost zero probability near the ion, those in the middle panel have a non-vanishing amplitude within the ionic potential. This can be understood by investigating the energetic position of the bound states of the atom-ion interaction localized in the ionic potential. In case they are near threshold, the

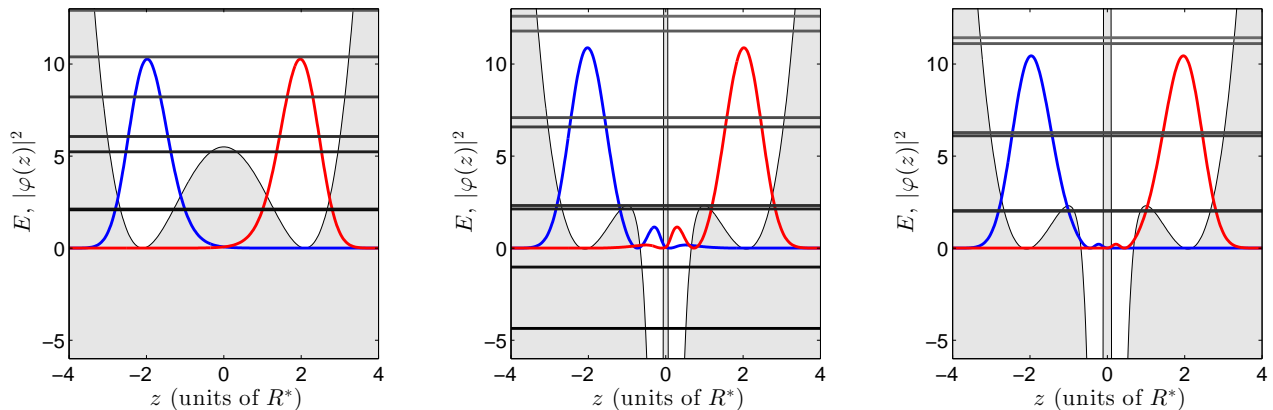


FIG. 2. Total potential (gray shaded area) together with the states  $|L\rangle$  and  $|R\rangle$  (blue and red line) and the single-particle eigenenergies (black horizontal lines) of the system without ion (left panel), with the ion in the internal state  $\omega = 29 (R^*)^{-4}$  and  $\gamma = 10\gamma_{\min}$  (middle panel), and with the ion in the internal state  $\omega = 80 (R^*)^{-4}$  and  $\gamma = \gamma_{\min}$  (right panel). Note that in the latter case the energy of the bound states is  $\epsilon_1 = -18.73E^*$  and  $\epsilon_2 = -15.54E^*$ .

eigenfunctions of the double well  $|L\rangle$  and  $|R\rangle$  obtain more and more a bound-state character which allows them to gain a finite amplitude in the ionic potential. We will see that in such a case the tunneling through the junction becomes possible.

### B. Theoretical Approach

The dynamical evolution of our many-body quantum system is determined via the numerically exact ab initio MCTDHB method [33]. Within this method, the many-body wave function is expanded in terms of bosonic number states  $|\mathbf{n}(t)\rangle$

$$|\psi\rangle = \sum_{\mathbf{n}|N} A_{\mathbf{n}}(t) |\mathbf{n}(t)\rangle \quad (6)$$

with the vector  $\mathbf{n} = (n_1, n_2, \dots)$  containing the occupations  $n_j$  of the single-particle function (SPF)  $|\Psi_j(t)\rangle$ . The symbol  $|N$  indicates that for a given  $\mathbf{n}$  the condition  $\sum_i n_i = N$  has to be fulfilled. Most importantly, here not only the expansion coefficients are time-dependent, but also the single-particle basis set  $\{|\Psi_j(t)\rangle\}_{j=1}^m$ . Note that in Sec. III  $m = 5$  and in Sec. IV  $m = 4$  time-dependent SPFs are used assuring the convergence of all results. By means of the Dirac-Frenkel variational principle [34, 35], the variational optimal temporal evolution of the many-body wave function is obtained. Thereby, the coefficients  $A_{\mathbf{n}}$  and the SPFs  $|\Psi_j\rangle$  are adapted to the many-body dynamics such that even with a small number of SPFs a maximal overlap of the ansatz (6) to the true many-body wavefunction is guaranteed. We refer for a detailed description of the method to Ref. [33]. Note that recently the method has been generalized to a multilayer (ML) structure to ML-MCTDHB allowing to treat even bosonic mixtures [36, 37].

In order to analyze the high-dimensional many-body wavefunction (6), we need to investigate relevant observables which allow us to understand mechanisms of the ongoing dynamics. At first, we use the one-body density (matrix)  $\rho(z, t) = \langle \hat{\Psi}^\dagger(z, t) \hat{\Psi}(z, t) \rangle$  ( $\rho(z, z', t) = \langle \hat{\Psi}^\dagger(z, t) \hat{\Psi}(z', t) \rangle$ ), defined via the field operators  $\hat{\Psi}^\dagger(z, t)$  and  $\hat{\Psi}(z, t)$ , which gives us information about the spatial arrangement of the ensemble. Furthermore, the spectral decomposition of the reduced one-body density matrix  $\rho(z, z', t) = \sum_j \lambda_j \Phi_j^*(z, t) \Phi_j(z', t)$  into the natural populations  $\lambda_j$  and the natural orbitals  $\Phi_j(z, t)$  provides useful information about the degree of fragmentation of the bosonic system [38] and can give valuable insights into the dynamical evolution of the system. Besides, the occupations  $f_k = \langle \hat{a}_k^\dagger \hat{a}_k \rangle$  and the coherences  $p_{kq} = \langle \hat{a}_k^\dagger \hat{a}_q \rangle$  (with  $k \neq q$ ) defined with respect to the eigenfunctions  $\phi_j(z)$  of the single-particle Hamiltonian  $\hat{h}$  introduced in Eq. (4) will be helpful quantities to assess the excitations during the dynamical evolution. We remark that in the literature  $\langle \hat{a}_k^\dagger \hat{a}_q \rangle$  are also referred to as *singlets* which are the matrix elements of the one-body reduced density matrix in the representation of  $\phi_j(z)$ .

### III. TUNNELING DYNAMICS

In the following, we analyze the evolution of the tunneling dynamics of the bosonic system for the two sets of quantum defect parameters  $\{\varphi_e^{\text{TR}} = 0.23\pi, \varphi_o^{\text{TR}} = -0.45\pi\}$  and  $\{\varphi_e^{\text{STR}} = 0.23\pi, \varphi_o^{\text{STR}} = 0.3\pi\}$  representing two internal states of the ion. Thereby, we identify and analyze in detail the many-body phenomena arising in the dynamics.

Let us begin with some simple considerations about the non-interacting case. Here the singlets  $\langle \hat{a}_k^\dagger \hat{a}_q \rangle$  oscillate

with the difference of the eigenfrequencies

$$\hbar\omega_{kq} = \epsilon_k - \epsilon_q \quad (7)$$

of the system. Note that the diagonal is therefore constant in time. Which of these frequencies are actually present in the dynamics depends on the initial state. In order to investigate tunneling dynamics, we can initialize all atoms in the state  $|\mathbf{L}(g=0)\rangle = (|\phi_3\rangle + |\phi_4\rangle)/\sqrt{2}$  which is localized in the left well. With this choice for the initial state we have  $|\langle\hat{a}_3^\dagger\hat{a}_3\rangle| = |\langle\hat{a}_4^\dagger\hat{a}_4\rangle| = |\langle\hat{a}_3^\dagger\hat{a}_4\rangle| = |\langle\hat{a}_4^\dagger\hat{a}_3\rangle| = \frac{N}{2}$ , while all other singlets vanish for all times. The dynamical evolution is here only driven by the phase of the coherence  $\langle\hat{a}_3^\dagger\hat{a}_4\rangle(t) = |p_{34}|e^{i\alpha_{34}(t)}$  which can be written as  $\alpha_{34}(t) = \omega_{34}t$ , thus, it increases linearly in time with  $\omega_{34}$  since the  $|\phi_j\rangle$  are eigenfunctions of  $\hat{h}$  [see Eq. (4)]. It is clear that the dominant frequency in the process is therefore  $\omega_{34}$  which is often called the *tunneling frequency*. In the dynamics, we would observe a tunneling from the one side of the double well to the other with period  $T_T = 2\pi/\omega_{34}$ .

Now taking the step to the interacting many-body system defined above, the above initial state would be difficult to realize experimentally and therefore we start from the equilibrated ground state in one well. This initial state is prepared by imaginary time propagation [39] without the ion but with an additional potential blocking the right well such that the atoms equilibrate into the left well only. The resulting many-body wave function is used as an initial state for the temporal evolution with the Hamiltonian (2) for both internal states of the ion. In Fig. 3, we show the resulting reduced one-body density exemplarily for  $N = 10$  for the TR (left panel) and the STR (right panel). This clearly demonstrates that we are able to access both dynamical regimes just by changing the model potential parameters (i.e., the atom-ion scattering lengths). In the dynamical process, we observe two main oscillations: a slow and a fast one. The slow oscillation in the TR occurs with approximately the above discussed single-particle tunneling frequency  $\hbar\omega_T \approx \epsilon_4 - \epsilon_3$  ( $T_T \approx 33.3 \hbar/E^*$ ). In contrast, in the STR, an incomplete tunneling is observable which occurs much faster than one would expect from the single-particle tunneling time  $T_T \approx 225.25 \hbar/E^*$ . Please note that the damping of the tunneling oscillations in the TR is already a first hint that a TMGP description is not adequate. The second fast oscillation mainly affects the density within the ionic potential. Such high frequency oscillations have also been observed in Ref. [24] and attributed to the population of other energetically higher states. Here, however, these are attributed to the additional length and energy scale introduced by the atom-ion interaction, as recently reported [19]. Their presence is already a first indicator that even a TMBH description would fail to describe the above dynamics in all their details.

Let us first analyze the so-called survival probability  $p_L(t) = \frac{1}{N} \int_{-\infty}^0 \rho(x, t) \chi [p_R(t) = \frac{1}{N} \int_0^{\infty} \rho(x, t) \chi]$ , which allows to quantify the tunneling process. In Fig. 3, we

show  $p_L$  (white line) and  $p_R$  (magenta line) for  $N = 10$  particles for the TR (left panel) and the STR (right panel). We observe that in the TR  $p_L$  nearly drops down to zero at  $t = 16.5 \hbar/E^*$  and returns back to about 90% of the initial population at  $t = 34 \hbar/E^*$ . This tunneling period still nicely corresponds to the non-interacting tunneling period  $T_T = 33.3 \hbar/E^*$ . The additional superimposed oscillations are clearly visible. We will see in the following that they consist of more than a single frequency. For longer times, the tunneling oscillation becomes damped and should reveal, at least in a TMBH description, collapse and revival behavior [27]. On the other hand, in the STR (right panel), we observe that only a very incomplete tunneling occurs such that no population inversion is reached. The survival probability  $p_L$  is only slightly decreased to about 90%. Furthermore, the amplitude of the fast oscillation on top of the self-trapping dynamics is much smaller compared to the TR and, here, the fast oscillation contains effectively only a single frequency as it will become apparent below.

In order to understand the dynamical evolution, it is helpful to investigate the contributing singlets of the system. As discussed for the non-interacting case, already the initial state is here of importance such that different preparation schemes could change the singlet contributions. Nevertheless, we should keep in mind that in the many-body scenario the (absolute) value of the singlets is not necessarily constant in time. In Fig. 4, we show the non-vanishing singlets of the two regimes under investigation again for the case of  $N = 10$  particles. It becomes clear that in the STR (right panel) the third and fourth single-particle eigenstates are the only ones which are visibly populated similarly to the single particle case. In contrast, in the TR (left panel), also the two bound states have, even in the initial state, a notable weight.

Moreover, we observe that, with respect to the non-interacting case, the occupations  $f_3$  and  $f_4$  show an oscillating behavior which is, thus, a consequence of the interactions. Using the equation of motion for the occupations [see Ref. [19]] we find, under the assumptions that only  $f_3$ ,  $f_4$  and  $p_{34} = |p_{34}|e^{i\alpha_{34}}$  contribute, that quantum correlations can be neglected and by choosing real-valued single particle basis functions and making the approximation  $|\phi_3|^2 \approx |\phi_4|^2$ , the evolution of the occupations is only possible as long as interactions are present, as it becomes evident from the following equations of motion:

$$\hbar \frac{f_3}{t} = 2U|p_{34}| \sin(2\alpha_{34}), \quad (8)$$

$$\hbar \frac{f_4}{t} = -2U|p_{34}| \sin(2\alpha_{34}). \quad (9)$$

We see that the populations are driven by the phase of the coherences and oscillate, as long as  $|p_{34}|$  is constant and  $\alpha_{34}$  linear in time as in the non-interacting case ( $\alpha_{34}(t) = \omega_{34}t$ ), as a cosine in time with frequency  $2\omega_{34}$ . Further, the evolutions of  $f_3$  and  $f_4$  possess oppo-

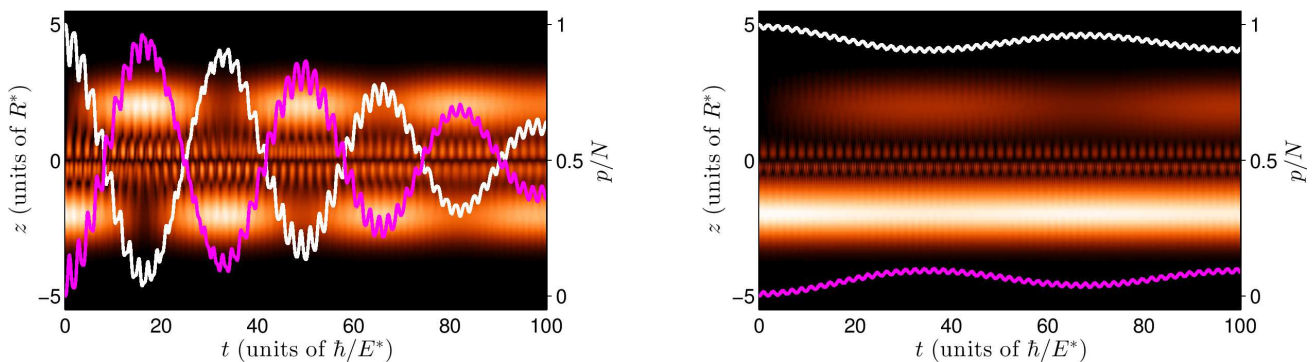


FIG. 3. Temporal evolution of the reduced one-body density  $\rho(z, t)$  and of  $p_L$  (white line) and  $p_R$  (magenta line) for  $N = 10$  particles for the TR (left panel) and the STR (right panel).

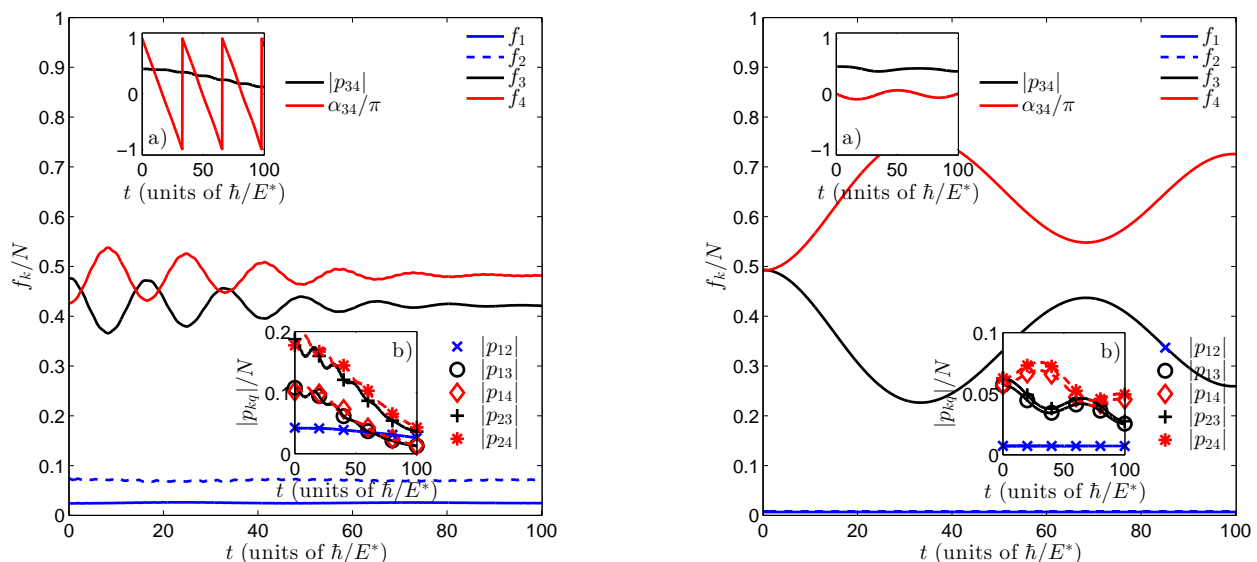


FIG. 4. Temporal evolution of the dominant occupations  $f_1$  (blue curve),  $f_2$  (dashed blue curve),  $f_3$  (black curve) and  $f_4$  (red curve) for  $N = 10$  particles in the TR (left panel) and the STR (right panel). Upper insets: The absolute value and the phase of the dominant coherence  $|p_{34}|$  (black curve) and  $\alpha_{34}$  (dashed red curve), respectively. Lower insets: The absolute value of the remaining coherences  $|p_{12}|$ ,  $|p_{13}|$ ,  $|p_{14}|$ ,  $|p_{23}|$ , and  $|p_{24}|$ .

site signs such that we can interpret Eqs. (8) and (9) as population transfer between the two states. Note that this process is not visible in the density evolution since  $|\phi_3|^2 \approx |\phi_4|^2$ . Similarly to the non-interacting case, the phase  $\alpha_{34}$  in the TR increases linearly in time (modulo  $2\pi$ ) with slope  $\omega_{34}$  as it is visible in Fig. 4 (upper insets) leading to clear cosine oscillations in  $f_3$  and  $f_4$ . In the STR, however, where the interaction strength is effectively larger [see Eq. (5)] the phase  $\alpha_{34}$  does not show a linear dependence on time anymore such that the dynamics can not be understood by Eqs. (8) and (9) only. Therefore, we need to employ, under the same assumptions as above, the equation of motion for  $p_{34}$  using the

equation of motion for the coherences

$$i\hbar \frac{p_{34}}{t} = [\epsilon_4 - \epsilon_3] p_{34} + 2U (f_3 - f_4) |p_{34}| \cos(\alpha_{34}). \quad (10)$$

The first term on the right hand side is the one which creates the linearly increasing phase  $\alpha_{34}$ . The second term comes into play if interactions are present and if a occupation imbalance  $f_3 - f_4$  between the two dominant modes exists. Since in the STR  $|f_3 - f_4|$  can become large, the impact of this non-linear term which couples the equation of motion of the occupations and the one of the coherence is much more pronounced.

The fast oscillation present in Fig. 3 can not be explained within this two mode analysis. Since we have already seen that both bound states are slightly populated, especially in the TR, we expect these bound states

to be the cause of the fast dynamics. Note that their occupations  $f_1$  and  $f_2$  are constant in time and can therefore not be related to the fast density oscillations visible in Fig. 3. What remains are the coherences between the bound states  $p_{12}$  as well as the coherences between the bound states and the two double well modes, that is,  $p_{13}, p_{14}, p_{23}, p_{24}$ . Their absolute values are shown in Fig. 4 (lower insets). Note that their phases increase linearly in time with the non-interacting energy difference  $\omega_{kq}$  [see Eq. (7)] as the corresponding slope (not shown). These energy differences can be observed in Fig. 2. In both cases  $\omega_{13} \approx \omega_{14} \equiv \omega_1$  and  $\omega_{23} \approx \omega_{24} \equiv \omega_2$ . Further, we can identify in the TR  $\omega_{12} \approx \omega_{23}$  (see Fig. 2 middle panel) such that effectively only two oscillation frequencies can be observed:  $\omega_1$  and  $\omega_2$ . They have the same order of magnitude  $\omega_1 \approx 2\omega_2$ . In contrast, in the STR, the frequencies  $\omega_1$  and  $\omega_2$  are comparably large due to the large energetic separation between the bound states and the other states such that we do not resolve their time scale in our figures (note that the numerical simulations cover these fast time scales). Therefore, only  $\omega_{12} \ll \omega_1 \approx \omega_2$  is visible in the shown dynamics. Thus, the fast superimposed oscillations result in the TR from five coherences, but they consist only of two comparable frequencies which explain the slight beating observable in Fig. 3. On the other hand, in the STR only a single coherence, namely  $p_{12}$ , is of importance and thus only a single frequency is visible, even though the other coherences do not vanish but evolve on a much faster time scale.

Up to now, we essentially investigated the interacting dynamics from a single particle point of view, namely the singlets, which do not provide information concerning the two (and more) particle correlations. Nevertheless, correlations are contained in the initial state as well as build-up during the dynamics because of the interaction. As an indicator for beyond mean-field physics we investigate in Fig. 5 the natural populations  $\lambda_j$  which certify the degree of fragmentation of the system [38]. Both in the tunneling and in the self-trapping regime, the initial state is nearly condensed ( $\lambda_1 \approx 1$ ), since the interaction strength used is only moderate. Only after intermediate times, other natural orbitals become populated. For the STR a depletion of 1% is reached in case of  $N = 10$  particles around  $t = 40 \hbar/E^*$ , whereas in the TR around  $t = 20 \hbar/E^*$ , thus much earlier than in the STR. Moreover, the depletion in the TR becomes much more pronounced. In both cases, we can even see the population of a third natural orbital. In order to understand which physical processes are taking place due to the occupation of the additional orbitals, we investigate also in Fig. 5 the natural orbitals themselves. We observe that the first natural orbital shows the behavior expected from the density of the atomic cloud: in the TR a clear periodic tunneling with frequency  $\omega_{34}$  and in the STR a strongly suppressed tunneling with the majority of the atoms remaining in the left well. Since the first natural orbital is still the dominant one, we can think of its

dynamics as corresponding to the GP solution. In this spirit, the second (and also higher) natural orbital can be understood as deviations from the GP solution induced by beyond mean-field correlations in the many-body wave function. Inspecting the second natural orbital, we see that it looks like the mirror image of the first natural orbital in both regimes. Therefore, it corresponds to the mode which would have been dominant in case the tunneling dynamics had started from the other side (i.e., the right well). The fact that such a mode becomes populated is a clear signature that many-body effects become important and that they can influence both the tunneling as well as the self-trapping behavior of the system. In addition to this, we observe that the third natural orbital is mainly localized within the ionic potential and can therefore be assigned to the above discussed contributions induced by the presence of the two bound states.

Let us emphasize here two important points: firstly, the presence of more than a single natural orbital with notable weight is a clear manifestation that a mean-field GP theory does not provide an accurate description of the system dynamics. In general, however, this does not rule out a multi-orbital mean-field, as e.g. the best mean-field approach [40], which means that the many-body state is accurately described by a single permanent  $|\mathbf{n}(t)\rangle$  [in contrast to Eq. (6)]. Secondly, the non-steady temporal evolution of the natural populations is a clear signature of the build-up of quantum correlations beyond a multi-orbital mean-field state [41], making the use of advanced methods such as MCTDHB indispensable.

In summary, despite the increasing level of many-body correlations over time in the dynamics of the bosonic Josephson junction, we can safely conclude that by manipulating the ion internal state a single trapped ion can indeed control the atomic flow through the junction. Furthermore, we note that to the best of our knowledge the connection between the dynamical population of the second natural orbital and the damping of the tunneling dynamics has not been made previously. To this aim, we briefly discuss in the next subsection an experimentally viable strategy to measure the degree of fragmentation and even the approximate dynamical shape of the natural orbitals.

### 1. Measuring the natural orbitals

The inspection of the dynamical evolution of the natural orbitals revealed that many-body correlations in the dynamics lead to the build-up of a second single-particle mode which is the mirror image of the first one. The excitation of this process, which seems as if the tunneling had started from the other side, effectively leads to an attenuation of the tunneling as well as the self-trapping behavior. Here we aim to provide a simple strategy to experimentally verify this intuitive picture for the effect of the quantum correlations. To this end, one needs to measure the reduced one-body density matrix and diag-

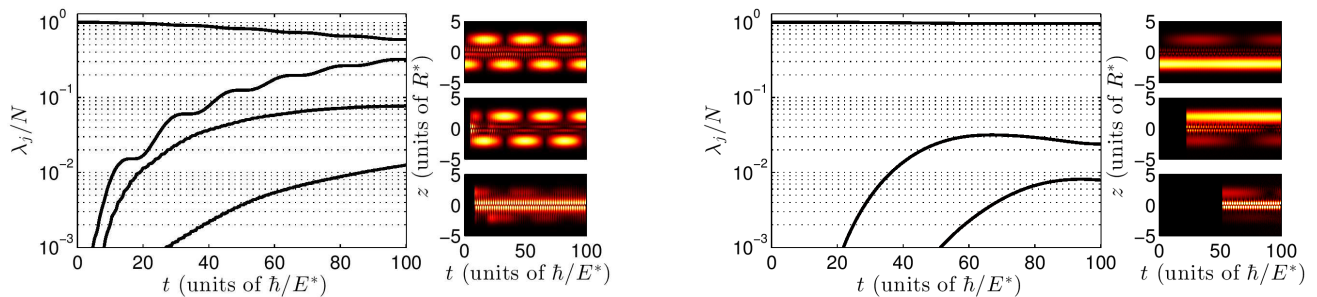


FIG. 5. Temporal evolution of the natural populations (main panel; black curves) together with the absolute value of the associated natural orbitals  $|\Phi_j(z,t)|$  [small insets; top ( $j=1$ ), middle ( $j=2$ ), bottom ( $j=3$ )] in the TR (left panel) and the STR (right panel). Further, note that  $\lambda_1 > \lambda_2 > \dots$  by definition. The natural orbitals are only plotted for times in which they are considerably occupied ( $\lambda_i > 10^{-3}$ ).

analyze it. In a two mode description ( $|L\rangle, |R\rangle$ ), we can write the reduced one-body density matrix as

$$\hat{\rho} = \frac{1}{2} (\mathbb{1} + \mathbf{a} \cdot \boldsymbol{\sigma}) = \frac{1}{2} \begin{pmatrix} 1 + a_z & a_x - ia_y \\ a_x + ia_y & 1 - a_z \end{pmatrix}, \quad (11)$$

with the Bloch vector  $\mathbf{a} = (a_x, a_y, a_z)$  and the vector of Pauli matrices  $\boldsymbol{\sigma} = (\sigma_x, \sigma_y, \sigma_z)$ . We note that the reduced one-body density matrix does not have to be pure, thus  $|\mathbf{a}| \leq 1$ . In this model, we only need to measure the entries of the Bloch vector  $a_i = \langle \sigma_i \rangle$  for  $i = x, y, z$ . Once those are known, the natural populations are given via diagonalization by

$$\lambda_{\pm} = \frac{1}{2} (1 \pm |\mathbf{a}|) \quad (12)$$

with their natural orbitals

$$|\Phi_{\pm}\rangle = \frac{1}{\sqrt{2|\mathbf{a}|(|\mathbf{a} \mp a_z|)}} [-(a_x - ia_y)|L\rangle + (a_z \mp |\mathbf{a}|)|R\rangle]. \quad (13)$$

Now we only need to answer the question how and if the Bloch vector components can be measured. Since the left and right modes have nearly no spatial overlap, the diagonal coefficients, thus  $a_z$ , can be determined from the density  $\rho(z, z)$  and define the population imbalance between the two wells. The off-diagonal terms, in contrast, contain the coherence of the left and the right part of the atomic cloud. These are accessible by time-of-flight measurements [42] which result in, neglecting interactions during the expansion, the Fourier transform to  $k$ -space of the reduced one-body density matrix  $\rho(k) = \frac{1}{2\pi} \int \langle z|z' \rangle \rho(z, z') e^{-ik(z-z')}$  (note that  $k$  and  $z$  are related by the ballistic expansion condition  $z(t) = \hbar tk/m$  [43]). Under the assumption that  $\langle z|L\rangle \approx \langle z - 2q|R\rangle$  ( $2q$  is the distance between the wells), equivalent to  $\langle k|L\rangle = e^{-2ikq} \langle k|R\rangle$  with  $|\langle k|L\rangle| = |\langle k|R\rangle| \equiv |\chi(k)|$ , we obtain

$$\rho(k) = |\chi(k)|^2 [1 + |c| \cos(2kq + \varphi)] \quad (14)$$

with  $a_x + ia_y = |c|e^{i\varphi}$ . Hence, by time-of-flight measurements we obtain the absolute value of the orbitals

in  $k$ -space modulated with a cosine where  $|c|$  is the amplitude or contrast of the modulation and  $\varphi$  its phase. Let us draw some conclusions from these considerations: first of all, we have seen that the length of the Bloch vector  $|\mathbf{a}|$  is a direct measure for the fragmentation of the system [see Eq. (12)]. Second, it limits the maximal population imbalance  $a_z \leq |\mathbf{a}|$  as well as the maximal contrast  $|c| \leq |\mathbf{a}|$  in the course of the tunneling in case fragmentation is present.

Furthermore, we note that Eq. (14) is not new in its form (see e.g. Ref. [44]) but only in its interpretation. Usually, the phase  $\varphi$  is the phase between the two modes of a Gross-Pitaevskii description, whereas here it is the phase of the off-diagonal matrix element of the reduced one-body density matrix. Additionally, the value of  $|c|$  is, in a GP description, directly connected to the diagonal elements of the one-body reduced density matrix, since in this case  $\hat{\rho}$  is constructed from a pure state. In a fully condensed situation those two cases coincide such that Eq. (14) represents a generalization to non-condensed (two-mode) many-body wave functions.

In summary, a measurement like the one of Refs. [21, 45] would be sufficient to estimate the full reduced one-body density matrix in a two-mode approximation such that, by using Eqs. (12) and (13), the natural populations, thus the level of fragmentation, and natural orbitals can be obtained. Let us note that this measurement scheme is not specific of the combined BEC-ion system investigated in this work, but it is quite general and can be applied to any atomic BJJ, for instance, the double well experiments of Refs. [21, 45, 46]. Even though the proposed measurement scheme is limited to two significantly populated natural orbitals, it should be sufficient for most of the experiments, since, typically, they are performed with a relatively large atom number and on limited time scales such that the contribution of orbitals higher than the second one can be safely neglected.



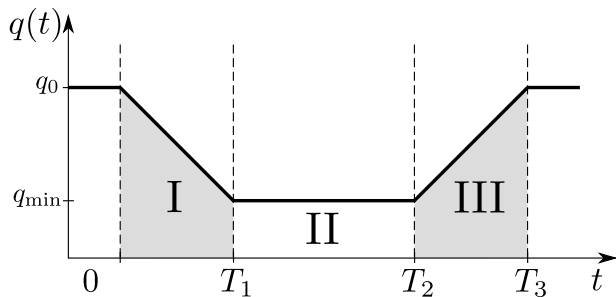


FIG. 6. Sketch of the time-dependent protocol for the double well separation used to create an entangled state between a single ion and an atomic ensemble. Initially, the dynamics is completely suppressed at large  $q = q_0$ . During the phase I, the tunneling dynamics is initiated such that it can evolve in the course of phase II. Finally, the process is reversed in phase III by taking the wells far apart.

#### IV. THE ENTANGLEMENT PROTOCOL

Let us investigate the possibility to generate an entangled state between the ion spin state and the atomic ensemble and let us denote the internal state of the ion leading to the TR with  $|\uparrow\rangle$  and the one leading to the STR with  $|\downarrow\rangle$ . Suppose now the ion to be initially prepared in a superposition of those two states ( $|\uparrow\rangle + |\downarrow\rangle$ ) and the atoms being prepared in the many-body ground state  $|\psi_L\rangle$  (or  $|\psi_R\rangle$ ) of the left (or right) well. The protocol to create a state of the form  $|\psi_R\rangle|\uparrow\rangle + |\psi_L\rangle|\downarrow\rangle$  was proposed in Ref. [25]. There, the main idea was to make the distance  $q$  between the two wells time-dependent. Starting at large  $q$  values, where tunneling is suppressed, the dynamics observed above, i.e tunneling and self-trapping, can be enabled by reducing  $q(t)$  to some fixed value  $q_{\min}$  such that they take place as discussed previously. After half of a tunneling period the reverse process is performed such that the initial large  $q$  value is restored leading finally to the desired (ideal) entangled state.

In order to verify whether such a protocol could still work if many-body correlations are taken into account, we also consider here a time-dependent  $q(t)$ . For the sake of simplicity, we use a linear time-dependence, as our goal is to show the working principle of the protocol. More precisely, we choose the following functional form also depicted in Fig. 6.

$$q(t) = \begin{cases} q_0 & t < 0 \\ q_0 - vt & 0 < t < T_1 \\ q_{\min} & T_1 < t < T_2 \\ q_{\min} + v(t - T_2) & T_2 < t < T_3 \\ q_0 & T_3 < t \end{cases} \quad (15)$$

We apply the protocol outlined above to both the TR and the STR separately given the linearity of the Schrödinger equation with respect to the ion internal state. The initial wave function in the left well is again

numerically computed without the ion, blocking the population in the right well with a step function, and executing imaginary time propagation. We use  $q_0 = 4.5R^*$ ,  $q_{\min} = 2.1R^*$  and  $|v| = 0.1R^*E^*/\hbar$ . The time  $T_1$  can be found via  $T_1 = (q_0 - q_{\min})/v$ , while the time  $T_2$  is determined by looking at the minimum of  $p_L$  in the TR, i.e., for the ion internal state  $|\uparrow\rangle$ .

#### A. The Dynamical Evolution

In Fig. 7, we show the temporal evolution of the density profile of the atomic cloud in the TR (left panel) and the STR (right panel) exemplary for  $N = 10$  using again  $m = 5$  SPFs. While for the ion internal state tuned to the TR most density is transported to the right side after the evolution, for the ion in the  $|\downarrow\rangle$  state, corresponding to the STR, most of the atoms remain trapped in the left well. The comparison with Fig. 3 shows that the dynamics occurring in phase II (i.e.,  $q(t) = q_{\min}$ ) nearly coincides with the primary dynamics for a constant  $q$ . Note, however, that tunneling already starts in phase I in the TR. Furthermore, we highlight that in both regimes the fast oscillations seen in Sec. III within the ionic potential are missing here which is a result of the initial state preparation. Instead, small dipole oscillations within each well excited by the ramping procedure are visible. Additionally, we show the survival probabilities  $p_{L,R}$  of the atoms in the left (white line) and right (magenta line) well for the TR (left panel) and the STR (right panel) in Fig. 7. We see that in the self-trapping case, the depletion of the left well population is only very small such that about 95% of the atoms stay in the left well. In the TR, we nearly achieve population inversion between the two wells at  $T_2$ , but since the dynamics cannot be instantaneously interrupted, about 12% of the atoms are in the left well at the end of the protocol. Although this is out of the scope of the present study, we note that higher transport efficiency can be attained by means of a compensating control pulse technique, that is, by optimally controlling the energy offset between the two wells [47].

In order to understand at which level of approximation the above dynamics can be described correctly, we investigate the natural populations as well as the singlets of the system. Firstly, we find that in the STR only a single natural orbital is considerably occupied ( $\lambda_1 \approx N$ ) meaning that the GP approximation is indeed fine. In contrast, in the TR, a second natural orbital becomes populated during the protocol up to  $\lambda_2 \approx 0.05N$  such that a mean-field description is not adequate, even though the initial state is almost perfectly condensed. Secondly, we checked the validity of the TMBH approach by the singlets populations  $f_k$ . Note that since the double well potential is now time-dependent, the single-particle Hamiltonian  $\hat{h}$  and its eigenfunctions become also time-dependent [see Eq. (4)], and therefore the creation and the annihilation operators  $\hat{a}_j^\dagger$  and  $\hat{a}_q$ , too. In

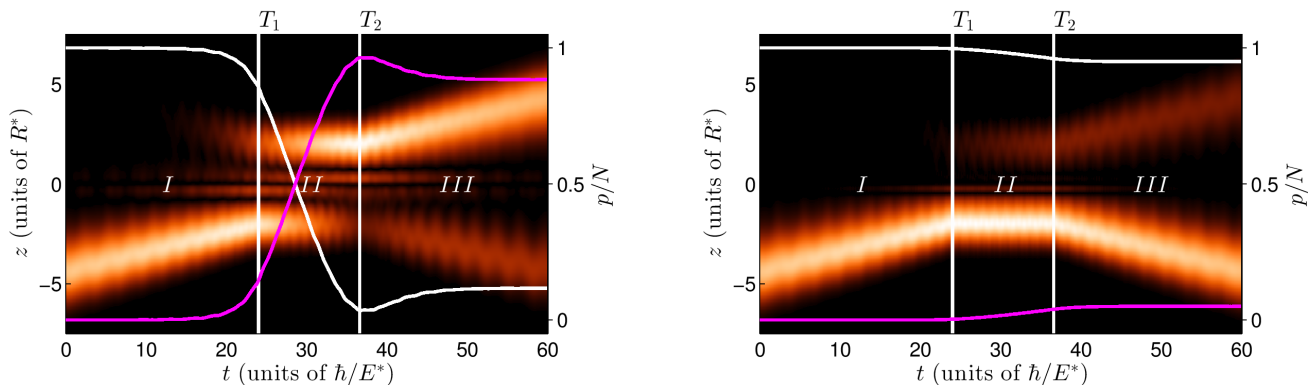


FIG. 7. Temporal evolution of the reduced one-body density  $\rho(z, t)$  and of  $p_L$  (white line) and  $p_R$  (magenta line) for  $N = 10$  particles using a time-dependent double well distance  $q(t)$  for the TR (left panel) and the STR (right panel). The times  $T_1$  and  $T_2$  are indicated by white vertical lines.

both regimes, we find that  $f_3 + f_4 \approx N$ , such that only the two modes  $[\phi_3(z, t)$  and  $\phi_4(z, t)]$  are sufficient for a correct theoretical description. We would like to emphasize, however, that only by choosing time-dependent mode functions the TMBH description of the protocol is valid, that is, time-independent mode functions would not lead to the correct BJJ dynamics.

Finally, let us mention that we have performed simulations of the protocol up to  $N = 100$  particles without any major qualitative difference. Only the degree of fragmentation reduces for increasing  $N$  due to the chosen scaling of the interaction strength with the particle number (i.e.  $gN = \text{const}$ ) such that the GP approximation is constantly improving for growing particle number.

### B. Fidelity of the Process

Finally, we want to evaluate quantitatively the efficiency of the entanglement protocol. The natural way to make such an assessment would be to compute the overlap integrals between the evolved states up to time  $T_3$  with the corresponding target states. This approach turns out to be computationally quite expensive due to the time-dependent SPF used in our method. In order to define a fidelity measure that contains more information about the system state than the density, we rely on the so-called Uhlmann fidelity [48–50]

$$F(t; \hat{\sigma}, \hat{\rho}_G) = \text{Tr} \left[ \sqrt{\sqrt{\hat{\rho}_G} \hat{\sigma}(t) \sqrt{\hat{\rho}_G}} \right] \quad (16)$$

Here  $\hat{\sigma}(t)$  is the density matrix of the system at time  $t$  and  $\hat{\rho}_G$  is the density matrix of the target state. In case of pure states ( $\hat{\sigma} = |\psi\rangle\langle\psi|$  and  $\hat{\rho}_G = |\psi_G\rangle\langle\psi_G|$ ) it is identical to the overlap integral  $F(t) = |\langle\psi_G|\psi\rangle|$ . In the present work we replace the density matrices  $\hat{\rho}_G$  and  $\hat{\sigma}$  with the corresponding one-body reduced density matrices. The derivation of Eq. (16) using  $\rho(z, z', t)$  is shown in App. A. We note that with this choice at least the

coherence, i.e. the off-diagonal elements of the reduced one-body density matrix, is taken into account, contrarily to a fidelity measure based on the atomic density (i.e.,  $p_L$  and  $p_R$ ) only.

For the STR, we choose as the target one-body density matrix the one corresponding to the initial state, while for the TR the one-body density matrix corresponding to the ground state of all atoms in the right well is used. In Fig. 8, the fidelity in dependence of time is shown for the TR (red line) and the STR (blue line). We see that for the STR the initial density matrix is recovered with a probability of more than  $F(T_3) \approx 97\%$  after the protocol. In the TR, we can prepare the opposite one-body density matrix with a fidelity of more than  $F(T_3) \approx 93\%$ . These values could still be improved, e.g. by optimally choosing the time  $T_2$ . Moreover, the whole ramping procedure could be fully optimized to reach a maximal fidelity by looking for an optimal shape of the separation  $q(t)$ . Nonetheless, even with the above non-optimized and simple strategy, the efficiency of the entanglement protocol is quite good. This shows that even without sophisticated control designs a very satisfactory and experimentally easy scheme can be accomplished in the laboratory with a high success probability.

Summarizing, we can state that when the ion is initially prepared in the state  $|\uparrow\rangle + |\downarrow\rangle$  both of the above processes would take place simultaneously such that we end up in the entangled state  $|\psi_R\rangle|\uparrow\rangle + |\psi_L\rangle|\downarrow\rangle$  with high fidelity.

### V. EXPERIMENTAL IMPLEMENTATION

The setup considered in this paper may be implemented in the laboratory by combining trapped ion technology with optical traps for atoms [26]. In recent years a number of experiments aimed at combining trapped ions and atoms have become available [1–3, 13] demonstrating the feasibility of this approach. Optical traps [21, 44, 51] or magnetic traps derived from micro-structured elec-

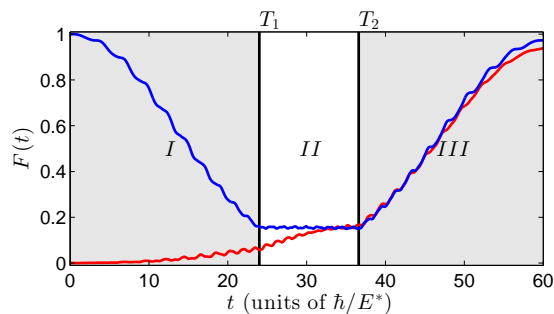


FIG. 8. Temporal evolution of the Uhlmann fidelity  $F(t)$ . (Red curve) Fidelity to find the atomic ensemble in the right well in the TR. (Blue curve) Fidelity to find the atomic ensemble in the left well in the STR.

tromagnets [46, 52] may be used to create atomic double well potentials with trapping frequencies in the kHz regime. The ion, in turn, may be trapped in a radio frequency Paul trap leading to very strong confinement. An interesting alternative is to trap the ion by optical potentials which was recently demonstrated [53, 54]. Employing such a setup may mitigate potential heating problems due to the time-dependent trapping field of the Paul trap [26, 55, 56]. The internal state of the ion may be probed by fluorescence detection and manipulated by external electromagnetic fields, whereas the atomic density and atom number can be obtained by time-of-flight analysis and absorption imaging. As a particular example we consider a  $^{171}\text{Yb}^+$  ion interacting with a BEC of  $^{87}\text{Rb}$  atoms [2]. For this combination, the typical length scale of the interaction is given by  $R^* = 375.31$  nm and  $E^*/h = 0.41$  kHz. Using  $q = 2.1R^*$  and  $b = 5.5E^*$ , as before, we get a trapping frequency of  $\omega_q = 2\pi \cdot 1.84$  kHz in each well. A transverse trapping frequency of  $\omega_\perp \sim 2\pi \cdot 25$  kHz allows us to reach the 1D regime with a 1D scattering length of  $a_{1D} = -389.3$  nm [57]. For this choice of parameters, we obtain, using  $N = 10$  particles,  $gN \approx 0.2E^*R^*$  as chosen in Sec. II A. The timescales in the manuscript correspond to  $\lesssim 40$  ms, for the considered atom-ion combination, such that we may expect coherence to be maintained in the ions internal state during the atomic tunneling. Heating of the ion during this period may be mitigated by using a large ion trap with large ion-electrode separation.

## VI. CONCLUSION

We presented a many-body study of an atomic BJJ interacting with a single trapped ion localized in the center of the junction. We found that the controlled switching of the BJJ by the ion is possible as in the original proposal [25], namely that the TR as well as the STR can be reached for fixed particle number and inter-atomic interaction strength even if all correlations are taken into account. In the TR, we found that correlations build-up

a second mode which decreases the population imbalance between the two wells leading to an “equilibration”, as already found within a TMBH approximation [27]. Additionally, a third mode with non-zero contribution is found, which is localized within the ionic potential, leading to fast oscillations on top of the tunneling dynamics. Similarly, the STR dynamics is harmed by the presence of a second mode, even though in this case the build-up of the many-body correlations takes place on a longer time scale. Also here fast oscillations are superimposed which are localized in the ionic potential, but they are less pronounced than in the TR. Interestingly, we find that in both regimes the second mode arising in the dynamics is the mirror image of the first one. This shows that the presence of correlations triggers the spatial mirror physical process which one would expect to be only present if the dynamics had started from the other side of the double well. In order to allow for an experimental confirmation of this behavior, we proposed a scheme to measure the natural populations and natural orbitals. The third mode, however, can be understood as a manifestation of the additional length and energy scale induced by the atom-ion interaction which highlights the necessity to describe the atom-ion interaction not simply by a repulsive contact interaction. In both cases, we can conclude that a GP description would not be able to capture the dynamics correctly. Even a multi-orbital mean-field ansatz could not reproduce the observed dynamics, since the build-up of a second and third mode is only possible by quantum correlations. Furthermore, although a TMBH description would give good approximative results, the dynamics within the ionic potential would be completely neglected. As a result, the above discussed fast oscillations in the left and right populations of the wells would not be traced in such a description.

With this knowledge, we examined to which extent the protocol proposed in Ref. [25] to create an entangled state between the ion and the atoms works. We were able to show that this protocol still represents a viable strategy for the creation of such an entangled state. Due to the relatively short tunneling time, quantum correlations are not able to drastically harm the dynamics, and therefore the protocol. In particular, it turns out that in the STR a single mode description, that is, GP, works quite well. In addition to this, we verified that the time-dependent dynamics of the protocol can be accurately well described by only two time-dependent mode functions, and therefore validating the theoretical approach used in Ref. [25]. The specific realization of the protocol chosen in this work is by no means optimal, but, nevertheless, we reached a fidelity of more than 90% and according to our considerations on the experimental implementation we can conclude that the control of the junction will be possible on experimental relevant time scales.

## VII. ACKNOWLEDGEMENTS

The authors thanks Sven Krönke and Valentin Bolsinger for many clarifying discussions. This work has been financially supported by the excellence cluster 'The Hamburg Centre for Ultrafast Imaging - Structure, Dynamics and Control of Matter at the Atomic Scale' of the Deutsche Forschungsgemeinschaft. R.G. gratefully acknowledges support by the EU via the ERC (Starting Grant 337638) and the DFG via SFB-TR/49.

### Appendix A: Derivation of the Uhlmann fidelity

Here we briefly explain how the Uhlmann fidelity can be evaluated by using, instead of the systems density matrix, the one-body reduced density matrix. Starting from Eq. (16), where now  $\hat{\sigma}(t)$  is the one-body reduced density matrix of the system at time  $t$  and  $\hat{\rho}_G$  is the one-body reduced density matrix of the target state, we can use the property of the Uhlmann fidelity, namely, it is preserved under a unitary transformation  $U$  of  $\hat{\rho}_G$  and  $\hat{\sigma}$

(thus  $F(t; \hat{\sigma}, \hat{\rho}_G) = F(t; U\hat{\sigma}U^\dagger, U\hat{\rho}_GU^\dagger)$ ):

$$F(t; \hat{\sigma}, \hat{\rho}_G) = \text{Tr} \left[ \sqrt{\sqrt{U\hat{\rho}_GU^\dagger}U\hat{\sigma}(t)U^\dagger\sqrt{U\hat{\rho}_GU^\dagger}} \right]. \quad (\text{A1})$$

Now choosing  $U$  as the transformation making  $\hat{\rho}_G$  diagonal, corresponding to the natural orbital representation, the inner square roots can easily be evaluated. With the natural occupations  $\lambda_k^G$ , the fidelity than can be written as

$$F(t; \sigma, \rho_G) = \text{Tr} \left[ \sqrt{W} \right]. \quad (\text{A2})$$

with the matrix  $W_{kq} = \sqrt{\lambda_k^G}C_{kq}(t)\sqrt{\lambda_q^G}$ , where  $C_{kq}(t) = U\hat{\sigma}(t)U^\dagger$  is  $\hat{\sigma}$  in the representation of the natural orbitals of  $\hat{\rho}_G$ . Again introducing a unitary matrix which now makes  $W$  diagonal  $W = U_W D_W U_W^\dagger$ , we can write the root of  $W$  as  $\sqrt{W} = U_W \sqrt{D_W} U_W^\dagger$ . Using the cyclic permutation of the trace, the fidelity turns out to be

$$F(t) = \sum_j \sqrt{w_j} \quad (\text{A3})$$

with  $w_j$  being the eigenvalues of  $W$ .

- 
- [1] A. T. Grier, M. Cetina, F. Oručević, and V. Vuletić, *Phys. Rev. Lett.* **102**, 223201 (2009).
  - [2] C. Zipkes, S. Palzer, C. Sias, and M. Köhl, *Nature* **464**, 388 (2010).
  - [3] S. Schmid, A. Härter, and J. H. Denschlag, *Phys. Rev. Lett.* **105**, 133202 (2010).
  - [4] R. Côté and A. Dalgarno, *Phys. Rev. A* **62**, 012709 (2000).
  - [5] Z. Idziaszek, T. Calarco, and P. Zoller, *Phys. Rev. A* **76**, 033409 (2007).
  - [6] R. Côté, V. Kharchenko, and M. D. Lukin, *Phys. Rev. Lett.* **89**, 093001 (2002).
  - [7] E. Gross, *Ann. Phys. (N. Y.)* **19**, 234 (1962).
  - [8] L. Landau and S. Pekar, *Zh. Eksp. Teor. Fiz.* **18**, 419 (1948).
  - [9] H. Fröhlich, *Adv. Phys.* **3**, 325 (1954).
  - [10] R. P. Feynman, *Phys. Rev.* **97**, 660 (1955).
  - [11] J. Kondo, *Prog. Theor. Phys.* **32**, 37 (1964).
  - [12] U. Bissbort, D. Cocks, A. Negretti, Z. Idziaszek, T. Calarco, F. Schmidt-Kaler, W. Hofstetter, and R. Gerritsma, *Phys. Rev. Lett.* **111**, 080501 (2013).
  - [13] A. Härter and J. Hecker Denschlag, *Contemp. Phys.* **55**, 33 (2014).
  - [14] J. Levinsen, M. M. Parish, and G. M. Bruun, *Phys. Rev. Lett.* **115**, 125302 (2015).
  - [15] R. S. Christensen, J. Levinsen, and G. M. Bruun, *Phys. Rev. Lett.* **115**, 160401 (2015).
  - [16] A. G. Volosniev, H.-W. Hammer, and N. T. Zinner, *Phys. Rev. A* **92**, 023623 (2015).
  - [17] L. A. P. Ardila and S. Giorgini, *Phys. Rev. A* **92**, 033612 (2015).
  - [18] J. M. Schurer, P. Schmelcher, and A. Negretti, *Phys. Rev. A* **90**, 033601 (2014).
  - [19] J. M. Schurer, A. Negretti, and P. Schmelcher, *New J. Phys.* **17**, 083024 (2015).
  - [20] A. Smerzi, S. Fantoni, S. Giovanazzi, and S. R. Shenoy, *Phys. Rev. Lett.* **79**, 4950 (1997).
  - [21] M. Albiez, R. Gati, J. Fölling, S. Hunsmann, M. Cristiani, and M. K. Oberthaler, *Phys. Rev. Lett.* **95**, 010402 (2005).
  - [22] S. Zöllner, H.-D. Meyer, and P. Schmelcher, *Phys. Rev. A* **74**, 053612 (2006).
  - [23] A. N. Salgueiro, A. de Toledo Piza, G. B. Lemos, R. Drumond, M. C. Nemes, and M. Weidemüller, *Eur. Phys. J. D* **44**, 537 (2007).
  - [24] K. Sakmann, A. I. Streltsov, O. E. Alon, and L. S. Cederbaum, *Phys. Rev. Lett.* **103**, 220601 (2009).
  - [25] R. Gerritsma, A. Negretti, H. Doerk, Z. Idziaszek, T. Calarco, and F. Schmidt-Kaler, *Phys. Rev. Lett.* **109**, 080402 (2012).
  - [26] J. Joger, A. Negretti, and R. Gerritsma, *Phys. Rev. A* **89**, 063621 (2014).
  - [27] G. J. Milburn, J. Corney, E. M. Wright, and D. F. Walls, *Phys. Rev. A* **55**, 4318 (1997).
  - [28] Z. Idziaszek, T. Calarco, P. S. Julienne, and A. Simoni, *Phys. Rev. A* **79**, 010702 (2009).
  - [29] B. Gao, *Phys. Rev. Lett.* **104**, 213201 (2010).
  - [30] Z. Idziaszek, A. Simoni, T. Calarco, and P. S. Julienne, *New J. Phys.* **13**, 083005 (2011).
  - [31] B. Gao, *Phys. Rev. A* **88**, 022701 (2013).
  - [32] M. Li, L. You, and B. Gao, *Phys. Rev. A* **89**, 052704 (2014).

- [33] O. E. Alon, A. I. Streltsov, and L. S. Cederbaum, Phys. Rev. A **77**, 033613 (2008).
- [34] P. A. M. Dirac, Math. Proc. Cambridge Philos. Soc. **26**, 376 (1930).
- [35] J. Frenkel, *Wave Mechanics*, 1st ed. (Clarendon Press, Oxford, 1934).
- [36] L. Cao, S. Krönke, O. Vendrell, and P. Schmelcher, J. Chem. Phys. **139**, 134103 (2013).
- [37] S. Krönke, L. Cao, O. Vendrell, and P. Schmelcher, New J. Phys. **15**, 063018 (2013).
- [38] O. Penrose and L. Onsager, Phys. Rev. **104**, 576 (1956).
- [39] R. Kosloff and H. Tal-Ezer, Chem. Phys. Lett. **127**, 223 (1986).
- [40] L. S. Cederbaum and A. Streltsov, Phys. Lett. A **318**, 564 (2003).
- [41] S. Krönke, *Correlated Quantum Dynamics of Ultracold Bosons and Bosonic Mixtures: the Multi-Layer Multi-Configuration Time-Dependent Hartree Method for Bosons*, Ph.D. thesis, Universität Hamburg (2015).
- [42] M. Greiner, C. A. Regal, J. T. Stewart, and D. S. Jin, Phys. Rev. Lett. **94**, 110401 (2005).
- [43] I. Bloch and W. Zwerger, Rev. Mod. Phys. **80**, 885 (2008).
- [44] R. Gati and M. K. Oberthaler, J. Phys. B At. Mol. Opt. Phys. **40**, R61 (2007).
- [45] T. Schumm, S. Hofferberth, L. M. Andersson, S. Wildermuth, S. Groth, I. Bar-Joseph, J. Schmiedmayer, and P. Krüger, Nat. Phys. **1**, 57 (2005).
- [46] T. Betz, S. Manz, R. Bücker, T. Berrada, C. Koller, L. Kazakov, I. E. Mazets, H.-P. Stimming, A. Perrin, T. Schumm, and J. Schmiedmayer, Phys. Rev. Lett. **106**, 020407 (2011).
- [47] I. Brouzos, A. I. Streltsov, A. Negretti, R. S. Said, T. Caneva, S. Montangero, and T. Calarco, (2014), arXiv:1412.6142.
- [48] A. Uhlmann, Reports Math. Phys. **9**, 273 (1976).
- [49] R. Jozsa, J. Mod. Opt. **41**, 2315 (1994).
- [50] M. A. Nielsen and I. L. Chuang, *Quantum Computation and Quantum Information* (Cambridge University Press, 2000).
- [51] S. Levy, E. Lahoud, I. Shomroni, and J. Steinhauer, Nature **449**, 579 (2007).
- [52] L. J. LeBlanc, A. B. Bardou, J. McKeever, M. H. T. Extavour, D. Jervis, J. H. Thywissen, F. Piazza, and A. Smerzi, Phys. Rev. Lett. **106**, 025302 (2011).
- [53] C. Schneider, M. Enderlein, T. Huber, and T. Schaetz, Nat. Photonics **4**, 772 (2010).
- [54] M. Enderlein, T. Huber, C. Schneider, and T. Schaetz, Phys. Rev. Lett. **109**, 233004 (2012).
- [55] M. Cetina, A. T. Grier, and V. Vuletić, Phys. Rev. Lett. **109**, 253201 (2012).
- [56] M. Krych and Z. Idziaszek, Phys. Rev. A **91**, 023430 (2015).
- [57] M. Olshani, Phys. Rev. Lett. **81**, 938 (1998).